Journal of Applied Mechanics and Technical Physics, Vol. 46, No. 5, pp. 670–676, 2005

LARGE-SCALE STREAMWISE VORTICES IN THE SUPERSONIC PART OF A PERMEABLE NOZZLE

V. N. Zaikovskii, S. P. Kiselev, and V. P. Kiselev

UDC 621.4:533.6

Large-scale streamwise vortices in the vicinity of a perforated wall in the supersonic part of the nozzle are studied. The governing effect of gas inflow through a perforated wall on origination and parameters of streamwise vortices is experimentally established.

Key words: *large-scale streamwise vortices, supersonic flow, nozzle, porous wall, gas inflow and outflow.*

Introduction. Nozzles with perforated walls in the supersonic part are widely used in wind tunnels for flow equalization and providing the transition through the velocity of sound [1]. The possibility of using porous inserts for passive control of the nozzle thrust has been considered recently [2]. Therefore, the flow structure in the nozzle was examined, and origination of large-scale streamwise vortices in the supersonic part of the nozzle was observed. Streamwise vortices were previously encountered in supersonic underexpanded jets [3] and in a plane supersonic flow past a backward-facing step [4]. They are called the Taylor–Görtler vortices, and their size is of the order of the boundary-layer thickness. Vortices of significantly greater size, depending on parameters of the gas injected through the porous insert, are considered in the present work. Note, this is not the only example of large-scale vortices observed in internal gas flows. Similar vortices were observed previously for plane and circular jets incident onto a submerged nozzle [5, 6]; they are formed in the subsonic part of the nozzle and then are entrained into the supersonic part.

Experimental Technique. The experimental studies were performed on the model shown in Fig. 1. The axisymmetric nozzle consists of two segments. The subsonic and supersonic parts of segment A are made of an impermeable material. The nozzle-throat diameter is $d_* = 38.4$ mm. Segment B is a replaceable supersonic bell with a permeable generating surface, which is attached to the exit section ($d_1 = 61.5$ mm) of segment A.

Two types of bells were used in experiments. The porosity of the first (metallic) bell is ensured by a system ($N = 1050$) of orifices 1.5 mm in diameter, which are uniformly distributed along the nozzle generatrix in 16 cross sections. The second bell is made of high-porous cellular carbon and provides uniform distributed inflow (or outflow) of the test gas.

The test gas was cold dry air with a temperature in the settling chamber $T_{0f} = 240$–270 K and a ratio of specific heats $\gamma = 1.4$. In the settling chamber, at the nozzle entrance, the pressure varied within 10 atm $\leqslant p_{0f} \leqslant$ 25 atm. The apex half-angle of the supersonic bell was $\delta = 8°$. The mean porosity in both cases was approximately identical ($m_1 \approx 20\%$). The medium parameters at the nozzle exit ($d_2 = 79$ mm) corresponded to the normal conditions ($T_\text{n} = 290$ K and $p_\text{n} = 1$ atm).

Mathematical Model of a Supersonic Gas Flow in the Nozzle with a Porous Insert. Let us consider a supersonic gas flow at $x > 0$ in the nozzle with a porous insert located at $x_1 < x < x_2$ (Fig. 2). The supersonic part of the nozzle is a cone described by the equation

$$r = r_*(1 + (x/r_*)\tan\delta). \tag{1}$$

Institute of Theoretical and Applied Mechanics, Siberian Division, Russian Academy of Sciences, Novosibirsk 630090; kiselev@itam.nsc.ru. Translated from Prikladnaya Mekhanika i Tekhnicheskaya Fizika, Vol. 46, No. 5, pp. 68–75, September–October, 2005. Original article submitted November 29, 2004.

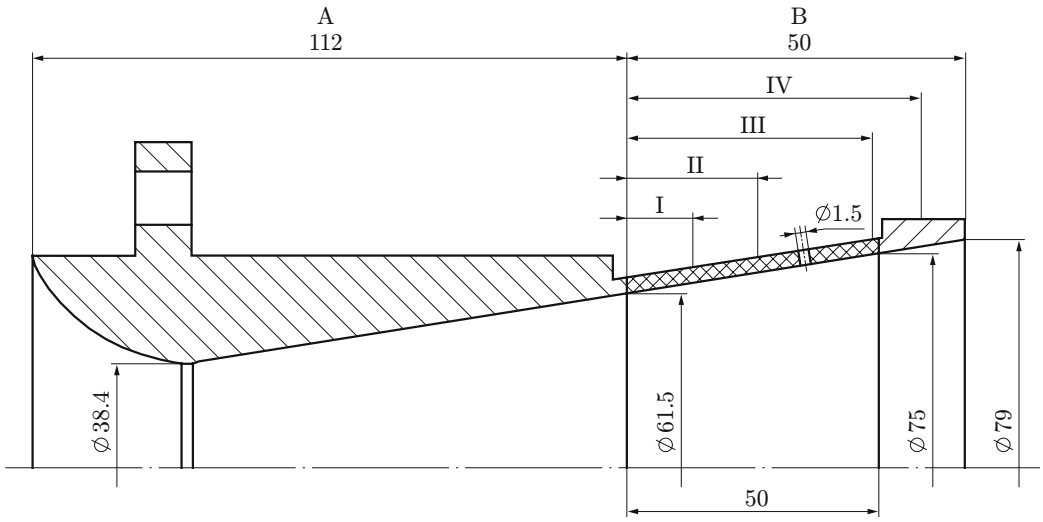

Fig. 1

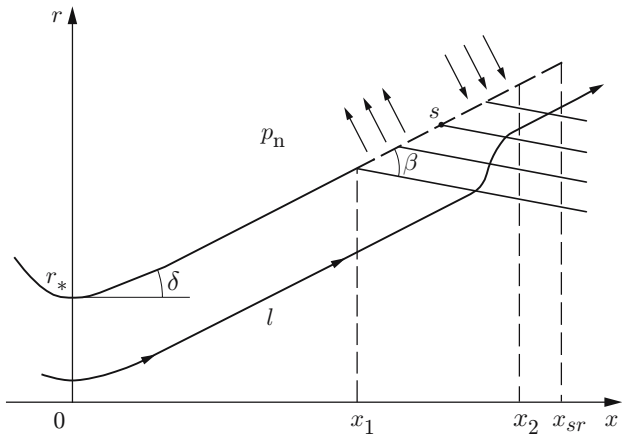

Fig. 2

The solution of the problem is constructed with the use of the perturbation theory. Denoting the free-stream parameters by the superscript 0, the parameters at the stagnation point by the subscript $0f$, and the parameters in the nozzle throat by the asterisk, we write the known isentropic formulas determining the gas flow in the nozzle in the zero approximation [7]:

$$\frac{T_*}{T_{0f}} = \frac{2}{\gamma+1}, \quad \frac{c_*}{c_{0f}} = \sqrt{\frac{2}{\gamma+1}}, \quad \frac{p_*}{p_{0f}} = \Big(\frac{2}{\gamma+1}\Big)^{\gamma/(\gamma-1)}, \quad \frac{\rho_*}{\rho_{0f}} = \Big(\frac{2}{\gamma+1}\Big)^{1/(\gamma-1)}, \quad \lambda = \frac{u^0}{c_*},$$

$$\frac{S}{S_*} = \Big(\frac{2}{\gamma+1}\Big)^{1/(\gamma-1)} \Big[\lambda\Big(1-\frac{\gamma-1}{\gamma+1}\lambda^2\Big)^{1/(\gamma-1)}\Big]^{-1}, \quad \frac{T^0}{T_*} = \frac{\gamma+1}{2}\Big(1-\frac{\gamma-1}{\gamma+1}\lambda^2\Big), \tag{2}$$

$$\frac{\rho^0}{\rho_*} = \Big(\frac{\gamma+1}{2}\Big)^{1/(\gamma-1)}\Big(1-\frac{\gamma-1}{\gamma+1}\lambda^2\Big)^{1/(\gamma-1)}, \quad \frac{p^0}{p_*} = \Big(\frac{\gamma+1}{2}\Big)^{\gamma/(\gamma-1)}\Big(1-\frac{\gamma-1}{\gamma+1}\lambda^2\Big)^{\gamma/(\gamma-1)}$$

[$S = \pi r^2(x)$ is the cross-sectional area of the nozzle]. If some portion of the nozzle $x_1 < x < x_2$ is replaced by a porous insert (Fig. 2), gas inflow (outflow) generates perturbations propagating inward the nozzle along the

characteristics. If the perturbations are small, the characteristics coincide with the Mach lines $\sin\beta = 1/\mathrm{M}$. As the flow is accelerated in the nozzle ($d\mathrm{M}/dx > 0$), we have $d\beta/dx < 0$, and the characteristics within one family do not intersect with each other. Below, we consider flows where the characteristics carrying the perturbations from the porous wall leave the nozzle before they reach the nozzle centerline (see Fig. 2, where x_{sr} is the nozzle-exit coordinate). In this case, we can neglect the term v_r/r in the continuity equation in calculating the perturbed flow. Then, the equations for perturbations take the form [1]

$$\begin{gathered}(1-\mathrm{M}^2)\,\frac{\partial u'}{\partial x}+\frac{\partial v'}{\partial r}=0, \qquad \frac{\partial u'}{\partial r}-\frac{\partial v'}{\partial x}=0,\\ p'=-\rho^0 u^0 u', \qquad \mathrm{M}=u^0/c^0, \qquad c^0=\sqrt{\gamma p^0/\rho^0},\end{gathered} \tag{3}$$

where $u = u^0 + u'$ is the velocity along the x axis, $v = v'$ is the velocity along the r axis, and $p = p^0 + p'$ is the pressure in the flow. The free-stream parameters indicated by the superscript "0" are described by formulas (2). In the present work, we consider a nozzle with a low angle of conicity $\delta \ll 1$, and this approximation is valid. The solution of Eqs. (3) is given by the formulas

$$v' \pm \sqrt{\mathrm{M}^2-1}\,u' = A_{1,2}, \qquad \sin\beta = \pm 1/\mathrm{M}, \tag{4}$$

where $A_{1,2}$ are constants for the first and second families of characteristics. The values of $A_{1,2}$ have to be determined from the boundary conditions. If the pore size is large enough to neglect the influence of viscosity on gas inflow (outflow) through the porous wall, Eqs. (4) are valid everywhere, including the porous portion of the nozzle wall. Using the first equation in (4) and assuming that $u' = 0$ in the pore and $v' = 0$ on the continuous portion of the porous wall, Nikol'skii derived the boundary condition on the porous segment [1]

$$u' = \frac{m_2}{m_1}\,\frac{v'}{\sqrt{\mathrm{M}^2-1}}, \qquad m_1 + m_2 = 1, \tag{5}$$

where m_1 is the porosity determined by the ratio of the area of orifices to the area of the porous portion of the nozzle.

Let p_n be the pressure in the outer volume to which gas outflow occurs. The inflow (outflow) velocity v' depends on the pressure difference $p - p_\mathrm{n}$ and on the structure of porosity. Below, we compare the calculated pressure on a permeable wall with experimental data for a metallic bell whose pores are orifices of diameter d of the order of the nozzle-wall thickness: $d \approx 1$ mm. Under these conditions, viscosity has almost no effect on gas inflow (outflow), and the pore can be considered as a micronozzle. Using the approximate formula for gas flow rate through the Laval nozzle [7] for low pressure differences $(p - p_\mathrm{n})/p_\mathrm{n} \ll 1$, we obtain expressions that describe gas outflow ($p > p_\mathrm{n}$)

$$v' = \frac{\xi m_1 c}{\sqrt{\gamma}}\sqrt{\frac{p-p_\mathrm{n}}{p}}, \qquad 0 < \frac{p-p_\mathrm{n}}{p} < \frac{1}{2} \tag{6}$$

and gas inflow ($p < p_\mathrm{n}$)

$$v' = \frac{\xi m_1 c_\mathrm{n}}{\sqrt{\gamma}}\sqrt{\frac{p_\mathrm{n}-p}{p_\mathrm{n}}}, \qquad 0 < \frac{p_\mathrm{n}-p}{p_\mathrm{n}} < \frac{1}{2}, \tag{7}$$

where $p = p^0 + p'$ is the pressure in the nozzle and p_n is the pressure in the ambient volume. The coefficient ξ was chosen from the condition of coincidence of the experimental and calculated values of pressure at a certain point on the porous wall: $\xi = 0.25$.

Calculation Results and Experimental Data. Figure 3 shows the experimental and calculated [by model (1)–(7)] static pressure on the wall versus the coordinate $p(x)$ on the porous portion of the nozzle with a pressure in the settling chamber $p_{0f} = 22$ atm. The circles, squares, and triangles correspond to data obtained in three experiments performed with an identical value of p_{0f}. The static pressure was measured at particular test points on the nozzle surface; in passing from one point to another, changes were made simultaneously in the x coordinate and azimuthal angle α. Thus, the points for pressure measurements were located along a spiral. The solid curve shows the dependence $p(x)$ calculated by the semi-empirical model (1)–(7) for the porous part; the dashed curve shows the dependence $p(x)$ calculated by formulas (1) and (2) for the nozzle without the porous insert. The calculations were performed for conditions used in experiments: $r_* = 19.2$ mm, $\delta = 8°$, and $m_1 = 0.18$.

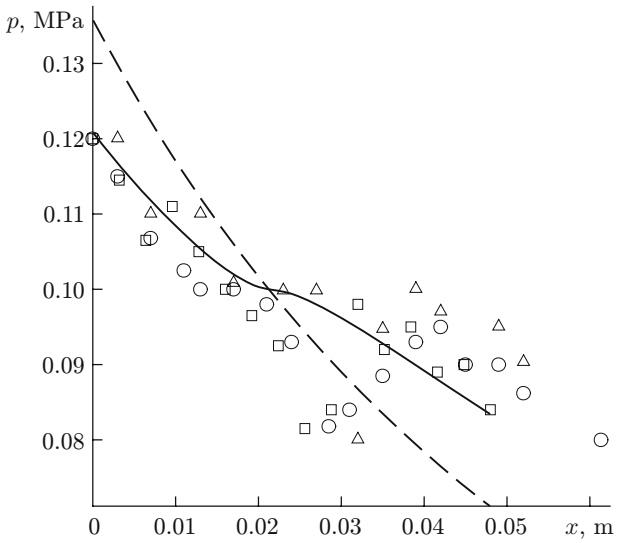

Fig. 3

The test gas was air with a temperature in the settling chamber $T_0 = 300$ K and a ratio of specific heats $\gamma = 1.4$. It follows from Fig. 3 that the experimental and numerical results are in good agreement in the region of gas outflow, where the pressure is $p > 1$ atm. In the region of gas inflow into the nozzle ($p < 1$ atm), the calculated pressures are significantly different from those measured in the experiment. This difference can be explained by the fact that the region where the gas-outflow mode changes to the gas-inflow mode involves the formation of large-scale vortices, which are entrained downstream (they are ignored in the present mathematical model). In the experiment, a shift along the angle α occurs in addition to the shift along the x axis in passing from one point to the next one, which leads to pressure oscillations in the presence of streamwise vortices.

To check this hypothesis, the distributions of static pressure p were experimentally measured at 20 test points over a certain part of the perimeter ($0 \leqslant \alpha \leqslant 120°$) for three cross sections of the perforated metallic bell: $x = 12.5$ (I), 25 (II), and 50 mm (III); see Fig. 1. Surface regions with both outflow ($p > p_\text{n} = 1$ atm) and inflow ($p < p_\text{n}$) of the test gas arise in the permeable supersonic segment owing to variation of pressure in the settling chamber p_{0f}. As it follows from data on longitudinal distributions $p(x)$ (Fig. 3), for a pressure in the settling chamber $p_{0f} = 22$ atm, the first cross section with pressure taps is located in the region of the transition (10 mm $< x <$ 20 mm) from outflow to inflow of the test gas. Subsequent cross sections with pressure taps are located further downstream, in the zone of gas inflow from the ambient medium.

Figures 4a, 4b, and 4c show the processed experimental data on the distribution of p for a certain part of the perimeter ($0 < \alpha < 120°$) in cross sections I, II, and III, respectively (see Fig. 1). The ordinate axis shows the deviations (in percent) of static pressure $\Delta\bar{p}$ in a given cross section of the permeable segment from the pressure at the corresponding point of the impermeable nozzle: $\Delta\bar{p} = (\tilde{p} - p)/\tilde{p}$, where $\tilde{p}$ is the static pressure at a test point of the permeable segment and p is the static pressure at the corresponding point of the impermeable segment. The abscissa axis shows the angular coordinates ($0 < \alpha < 120°$) of the pressure taps over the perimeter of the cross sections (I, II, and III). Insignificant periodic deviations of the parameter $\Delta\bar{p}$ ($\pm 1.5\%$) are noted in cross section I on the inner surface of the permeable segment, which indicates the existence of the region where swirled streamwise vortices are formed (see Fig. 4a). Paired large-scale vortices are completely developed and formed further downstream between cross section I and cross section II. The characteristic periodic change in the parameter $\Delta\bar{p}$ within significant limits: $\pm 4\%$ (Fig. 4c), i.e., the presence of two maximums and two minimums, allows us to argue that there exist two pairs of streamwise vortices on this part of the inner surface ($0 < \alpha < 120°$). The qualitative pattern of these vortices is shown in Fig. 4d, where the pluses and minuses refer to divergence and convergence points of secondary gas flows generated by vortices on the nozzle wall. As only an arbitrarily chosen third of the cross-sectional contour is considered, we can conclude that six pairs of vortices are uniformly distributed over the

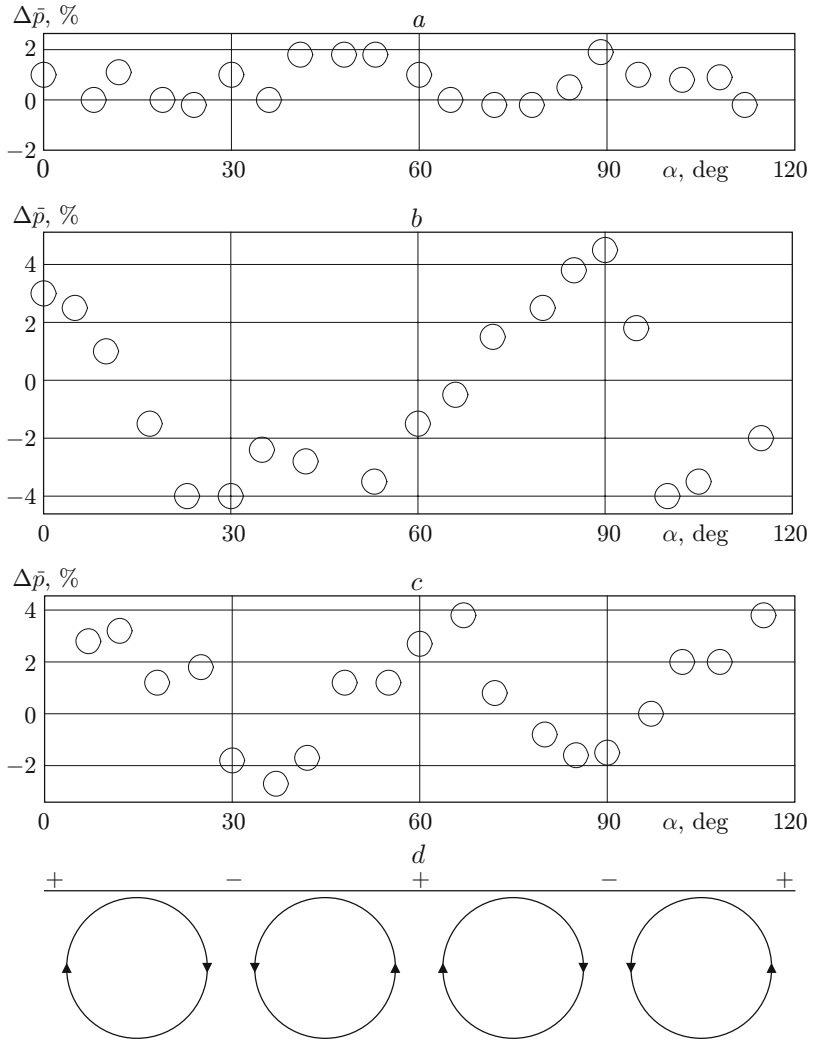

Fig. 4

perimeter of the permeable segment ($0 < \alpha < 360°$). Between segment II and segment III, the vortex diameter increases in accordance with the increase in the open area of the nozzle, which leads to a decrease in $\Delta\bar{p} \approx 3\%$ (Fig. 4c). At the exit of the perforated metallic segment, there is a developed steady system of six pairs of large-scale counter-rotating streamwise vortices of diameter $d_v \approx 15$ mm.

Figure 5 shows the distribution of the dimensionless difference in static pressure $\Delta\bar{p}$ over one third ($0 < \alpha < 120°$) of the perimeter in cross section IV ($x = 58$ mm) of the permeable segment made of high-porous cellular carbon. It is seen that uniformly distributed inflow of the test gas introduces significant qualitative and quantitative changes in the flow structure in the inner volume of the supersonic bell. The maximum values of $\Delta\bar{p}$ increase by a factor of 2: $\pm 8\%$ (Fig. 5a). A maximum of $\Delta\bar{p}$ is noted in the central part of the cross section, and minimums of $\Delta\bar{p}$ are observed at the periphery. Based on such a distribution of experimental data, the model accepted predicts only one pair of vortices in cross section IV ($0 < \alpha < 120°$); the qualitative pattern of these vortices in the vicinity of the nozzle wall is shown in Fig. 5b. In this case, only three pairs of swirled structures with a local vortex diameter $d_v \approx 26$ mm can be uniformly located over the entire perimeter of the inner surface of the permeable segment.

It follows from the above-described experimental and theoretical results than large-scale streamwise vortices are formed in the gas flow during the transition from gas outflow to gas inflow through the porous insert located in the supersonic part of the nozzle. The size of vortices is much greater than the boundary-layer thickness and

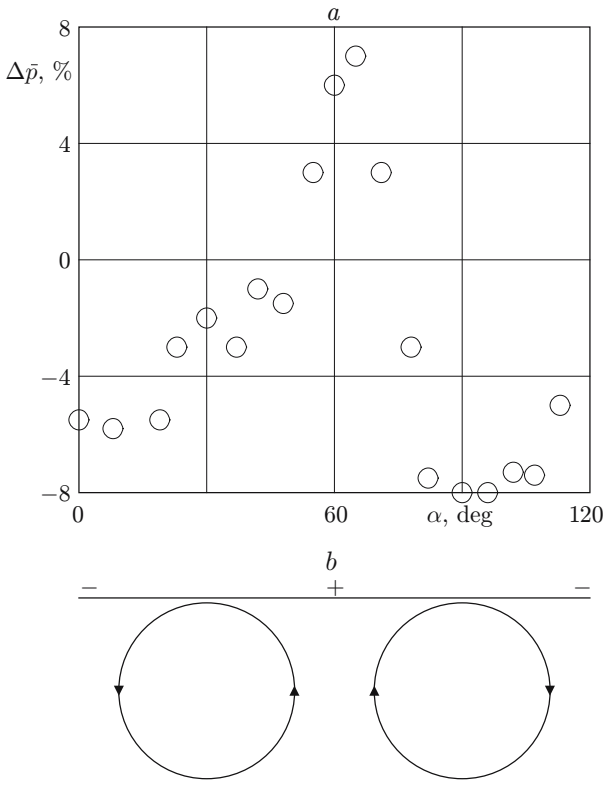

Fig. 5

depends on the structure of the porous segment. In particular, in the case of uniformly distributed porosity, which is observed for a wall made of high-porous cellular carbon, the vortex size is two times greater than that for a wall with rows of pressure taps. This is the significant difference of these vortices from the streamwise vortices observed in [3, 4], whose size was commensurable with the boundary-layer thickness. This difference seems to be related to the fact that gas inflow through the porous wall destroys the laminar flow in the boundary layer and entrains portions of the gas with a low streamwise velocity to significant distances from the wall; as a result, the size of the region with the velocity gradient of the gas increases.

Let us consider the mechanism of formation of streamwise vortices in this case. The qualitative pattern of the gas flow in a nozzle with a porous wall is shown in Fig. 2, where the point s separates the regions of gas outflow and inflow. The change in flow regimes generates positive curvature on the streamline l, which acquires the maximum value in the vicinity of the point s. As the gas flow near the wall has a negative gradient $\partial u/\partial r < 0$, this breaks the equilibrium between the pressure gradient and the centrifugal force [8]. As a result, instability starts to develop in the flow, which is finalized by formation of large-scale streamwise vortices.

It was noted above that similar paired counter-rotating large-scale streamwise vortices arise owing to interaction of a subsonic jet ($M \approx 0.4$) with the surface of the subsonic part of the nozzle [5, 6]. Then, these vortices are entrained downstream and enter the supersonic part of the nozzle, where their intensity decreases owing to expansion of vortex tubes. Formation of vortices is related to the curvature of streamlines caused by jet impingement on the subsonic part of the nozzle.

Thus, the experiments performed revealed large-scale streamwise vortices formed in the supersonic part of the nozzle owing to gas inflow-outflow through a porous wall.

REFERENCES

1. G. L. Grozdovskii, A. A. Nikol'skii, G. P. Svishchev, and G. I. Taganov, *Supersonic Gas Flows in Perforated Boundaries* [in Russian], Mashinostroenie, Moscow (1967).
2. V. N. Zaikovskii, V. P. Kiselev, S. P. Kiselev, et al., "Effect of a porous insert in the supersonic part of the nozzle in changes in the nozzle thrust," *Dokl. Ross. Akad. Nauk*, **401**, No. 4, 479–482 (2005).
3. V. I. Zapryagaev and A. V. Solotchin, "Spatial flow structure at the initial part of a supersonic underexpanded jet," Preprint No. 23-88, Inst. Theor. Appl. Mech., Sib. Div., Acad. of Sci. of the USSR, Novosibirsk (1988).
4. A. A. Zheltovodov, E. H. Shülein, and V. N. Yakovlev, "Development of a turbulent boundary layer under conditions of mixed interaction with shock waves and expansion waves," Preprint No. 28-83, Inst. Theor. Appl. Mech., Sib. Div., Acad. of Sci. of the USSR, Novosibirsk (1983).
5. V. N. Zaikovskii and B. M. Melamed, "Vortex flows in SRM nozzles," in: *Stability of Homogeneous and Heterogeneous Fluid Flows,* Proc. VII Int. Conf. (Novosibirsk, April 12–14, 2000), Inst. Theor. Appl. Mech., Sib. Div., Russian Acad. of Sci., Novosibirsk (2000), pp. 183–186.
6. B. M. Melamed and V. N. Zaikovskii, "An experimental study of vortex structures in gas dynamic duct with swiveling nozzle," in: *Proc. of the IX Int. Conf. on the Method Aerophysical Research* (Novosibirsk, June 29–July 3, 1998), Part 3, Inst. Theor. Appl. Mech., Sib. Div., Russian Acad. of Sci., Novosibirsk (1998), pp. 189–192.
7. L. G. Loitsyanskii, *Mechanics of Liquids and Gases*, Pergamon Press, Oxford-New York (1966).
8. L. D. Landau and E. M. Lifshits, *Course of Theoretical Physics*, Vol. 6: *Fluid Mechanics*, Pergamon Press, Oxford-Elmsford, New York (1987).